PET Imaging of Colorectal Cancer in Xenograft-Bearing Mice by Use of an ^{18}F-Labeled T84.66 Anti–Carcinoembryonic Antigen Diabody

Weibo Cai[1], Tove Olafsen[2], Xianzhong Zhang[1], Qizhen Cao[1], Sanjiv S. Gambhir[1,3], Lawrence E. Williams[4], Anna M. Wu[2], and Xiaoyuan Chen[1]

[1]Molecular Imaging Program at Stanford (MIPS) and Bio-X Program, Department of Radiology, Stanford University School of Medicine, Stanford, California; [2]Crump Institute for Molecular Imaging, Department of Molecular and Medical Pharmacology, David Geffen School of Medicine, UCLA, Los Angeles, California; [3]Department of Bioengineering, Stanford University School of Medicine, Stanford, California; and [4]Division of Radiology, City of Hope National Medical Center, Duarte, California

In this study, we investigated the ^{18}F-labeled anti–carcinoembryonic antigen (CEA) T84.66 diabody, a genetically engineered noncovalent dimer of single-chain variable fragments, for small-animal PET imaging of CEA expression in xenograft-bearing mice. **Methods:** ^{18}F labeling of the anti-CEA T84.66 diabody (molecular mass, 55 kDa) was achieved with *N*-succinimidyl-4-^{18}F-fluorobenzoate (^{18}F-SFB). The biodistribution of the ^{18}F-fluorobenzyl-T84.66 diabody (^{18}F-FB-T84.66 diabody) was evaluated in athymic nude mice bearing subcutaneous LS 174T human colon carcinoma and C6 rat glioma tumors. Serial small-animal PET imaging studies were performed to further evaluate in vivo targeting efficacy and pharmacokinetics. **Results:** Radiolabeling required 35 ± 5 (mean ± SD) min starting from ^{18}F-SFB, and the tracer ^{18}F-FB-T84.66 diabody was synthesized with a specific activity of 1.83 ± 1.71 TBq/mmol. The decay-corrected radiochemical yield was 1.40% ± 0.16% (n = 4), and the radiochemical purity was greater than 98%. The radioimmunoreactivity was 57.1% ± 2.0%. The ^{18}F-FB-T84.66 diabody showed rapid and high tumor uptake and fast clearance from the circulation in the LS 174T xenograft model, as evidenced by both small-animal PET imaging and biodistribution studies. High-contrast small-animal PET images were obtained as early as 1 h after injection of the ^{18}F-FB-T84.66 diabody, and only a background level of activity accumulation was found in CEA-negative C6 tumors. The tracer exhibited predominantly renal clearance, with some activity in the liver and spleen at early time points. **Conclusion:** The ^{18}F-labeled diabody represents a new class of tumor-specific probes for PET that are based on targeting cell surface antigen expression. The ^{18}F-FB-T84.66 diabody can be used for high-contrast small-animal PET imaging of CEA-positive tumor xenografts. It may be translated to the clinic for PET of CEA-positive malignancies.

Received Jun. 27, 2006; revision accepted Aug. 23, 2006.

For correspondence or reprints contact: Xiaoyuan Chen, PhD, Molecular Imaging Program at Stanford (MIPS) and Bio-X Program, Department of Radiology, Stanford University School of Medicine, 1201 Welch Rd., P095, Stanford, CA 94305-5484.
E-mail: shawchen@stanford.edu

Key Words: carcinoembryonic antigen (CEA); T84.66 diabody; ^{18}F; small-animal PET; colorectal cancer

J Nucl Med 2007; 48:304–310

Many monoclonal antibody (mAb) products have been approved for clinical use, and dozens more are currently undergoing clinical evaluation (*1,2*). In addition, mAbs have been conjugated to active moieties, such as drugs, toxins, or radionuclides (*1*). Intact antibodies can be used for radioimmunotherapy or targeted delivery of therapeutic agents because they exhibit high tumor uptake and retention. However, for imaging purposes, radiolabeled intact mAbs are not the optimal choice because of their prolonged persistence in the circulation, which leads to high background activity in the blood and normal tissues. Instead, researchers have turned to enzymatically derived antibody fragments or genetically engineered fragments with optimized targeting and pharmacokinetic properties (*3*). Single-chain variable fragments (scFvs) with a molecular mass of 25 kDa are cleared very rapidly from the circulation, but they exhibit poor tumor retention because they are monovalent. Bivalent antibody fragments with intermediate molecular masses possess more ideal tumor-targeting characteristics, including rapid tissue penetration, high target retention, and rapid blood clearance. In particular, the diabody format (a dimer of scFvs; molecular mass, 55 kDa) has been evaluated for targeting in several tumor antigen systems and has demonstrated rapid tumor localization (*4–7*) and high-contrast imaging (*8,9*). SPECT imaging of tumor neovascularization with an ^{123}I-labeled antifibronectin extra-domain B scFv dimer in cancer patients has demonstrated the potential of engineered antibodies as novel radiotracers (*10*). SPECT with a ^{123}I-labeled, slightly larger antibody fragment, an anti–carcinoembryonic antigen (CEA) minibody (scFv-C_H3

dimer; molecular mass, 80 kDa), was recently reported to be able to delineate lesions in presurgical colorectal cancer patients, including 3 lesions that were not visible by CT (*11*).

CEA is a cell surface glycoprotein (molecular mass, 180 kDa) that is expressed during the development of the fetal gut (*12*). Subsequently, the expression of CEA is minimal and is limited to the lumen of the colon in adult humans. However, the development of colorectal cancer is almost uniformly associated with high-level reexpression of CEA (*13*). Furthermore, cleavage by phospholipases results in the release of CEA into surrounding tissues and the circulation, making serum CEA a useful marker for recurrence and response to treatment. CEA expression is also elevated in a substantial proportion of carcinomas of the lungs, breasts, pancreas, ovaries, and uterus and in medullary thyroid carcinomas (*13*). ^{99m}Tc-Arcitumomab (CEA-Scan; Immunomedics, Inc.) is a U.S. Food and Drug Administration–approved agent for whole-body planar and SPECT imaging of CEA expression.

We previously described the assembly of an anti-CEA diabody (scFv dimer), derived from the murine anti-CEA T84.66 mAb, by joining the light- and heavy-chain variable regions of the antibody with an 8-amino-acid-residue linker (*5*). The resulting homodimeric protein is a small, bivalent antibody fragment (approximately 55 kDa) that retains excellent antigen-binding properties (*5*). Biodistribution studies of a radioiodinated anti-CEA T84.66 diabody demonstrated that maximum tumor uptake occurred within 2 h after intravenous administration into CEA-positive LS 174T human colon cancer xenograft–bearing mice and that the protein was cleared from the circulation with a terminal half-life of 2.9 h (*5*). Small-animal PET imaging with a ^{124}I-labeled T84.66 diabody showed specific localization to the CEA-positive xenografts and relatively low activity elsewhere in the mice (*8*). Low levels of normal tissue activity, especially in the abdominal region, resulted in high-contrast images at 18 h for the ^{124}I-labeled T84.66 diabody.

Despite the success of the ^{124}I-labeled T84.66 diabody in the preclinical imaging of tumor CEA expression, we postulated that an ^{18}F-labeled diabody is potentially more suitable than ^{124}I-labeled engineered antibodies. In particular, for clinical development, ^{18}F offers the advantages of broad availability, a higher positron yield (nearly 100%, compared with 23% for ^{124}I), and a short half-life (109.7 min), which is better suited for routine clinical use. Furthermore, the physical half-life of ^{18}F is well matched to the biologic targeting and clearance kinetics of diabodies. We previously described an imaging figure of merit (IFOM), a measure of how rapidly a statistically significant tumor image can be acquired (*14*). IFOM values were calculated for combinations of different radionuclides with various engineered antibody fragments [scFv, diabody, minibody, F(ab′)$_2$, and intact antibody] on the basis of murine biodistribution data. We predicted that the diabody should provide the best vehicle for ^{18}F and that optimal imaging should occur at 1–2 h after injection (*14*). In the present work, we directly address the feasibility of early PET with an ^{18}F-labeled anti-CEA diabody.

MATERIALS AND METHODS

Unless otherwise specified, all chemicals were of analytic grade and were commercially available.

Production and Purification of T84.66 Diabody

High-level mammalian expression of the T84.66 diabody, purification, and characterization were reported in detail previously (*15*). Briefly, the diabody was secreted from NS0 murine myeloma cells with a pEE12 expression vector containing a cytomegalovirus promoter. Cell culture supernatants were cleared and subjected to sequential chromatography on anion exchange and hydroxyapatite columns, resulting in diabody preparations of greater than 98% purity (Figs. 1A and 1B).

Cell Lines and Xenografts

The LS 174T human colorectal carcinoma cell line (CL-188; high CEA expression) and the C6 rat glioma cell line (CCL-107; negative for CEA expression) were obtained from the American Type Culture Collection and maintained under standard conditions (*8,16*). All animal experiments were performed under a protocol approved by the Stanford University Administrative Panel on Laboratory Animal Care. The LS 174T colorectal cancer model was established by subcutaneous injection of 2×10^6 cells into the left front leg of female athymic nude mice (Harlan), and 5×10^6 cells were injected for the C6 tumor model. The mice were used for biodistribution and small-animal PET imaging studies when the tumor volume reached 100–300 mm^3 (10–15 d after inoculation for both tumor models).

Radiolabeling

N-Succinimidyl-4-^{18}F-fluorobenzoate (^{18}F-SFB) was synthesized as previously reported with high-performance liquid chromatography (HPLC) purification (*17–19*). Recently, we incorporated ^{18}F-SFB synthesis into a commercially available synthetic module (TRACERlab FX$_{FN}$; GE Healthcare) with full lead shielding and automatic control. The detailed procedure will be reported elsewhere. ^{18}F-SFB was added to the T84.66 diabody (300 μg) in 800 μL of

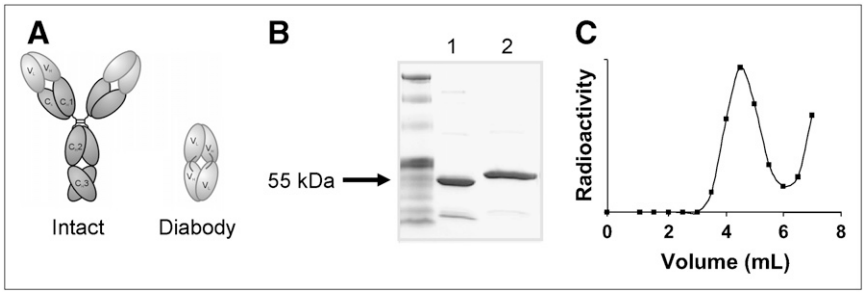

FIGURE 1. (A) Schematic structures of intact mAb and engineered diabody. (B) Sodium dodecyl sulfate–polyacrylamide gel electrophoresis of T84.66 diabody. Lane 1: nonreduced; lane 2: reduced. (C) Size exclusion column chromatography profile of ^{18}F-FB-T84.66 diabody. Nonreactive ^{18}F-SFB (eluting after 6 mL) was well separated from radiotracer. Fractions from 3.5 to 5 mL were used for in vitro and in vivo experiments.

sodium borate buffer (50 mM, pH 8.5). The reaction mixture was gently mixed at 40°C for 30 min. Final purification was accomplished by size exclusion chromatography (PD-10 column; GE Healthcare) with phosphate-buffered saline (pH 7.4) as the mobile phase. The purified ^{18}F-fluorobenzoyl-T84.66 diabody (^{18}F-FB-T84.66 diabody) was passed through a 0.22-μm Millipore filter (Millipore Corp.) for in vivo applications. Immunoreactivity was determined by incubation of the ^{18}F-FB-T84.66 diabody with an excess number of LS 174T cells or C6 cells. After 2 h at 4°C with constant shaking, the vials were centrifuged at 1,000 rpm, and the activities in the supernatant and the pellet were measured with a γ-counter (GMI, Inc.).

Biodistribution Studies

Female athymic nude mice bearing LS 174T tumors were each injected via the tail vein with about 0.37 MBq of the ^{18}F-FB-T84.66 diabody in 100 μL of phosphate-buffered saline. The mice were sacrificed and dissected at 1, 2, 4, and 6 h after injection. Blood, tumors, major organs, and tissues were collected and weighed wet. The radioactivity in the tissues was measured with the γ-counter. The results are presented as percentage injected dose per gram (%ID/g). For each mouse, the radioactivity in the tissue samples was calibrated against a known quantity of the injected dose and normalized to a mouse body weight of 20 g. Values were expressed as mean ± SD for 4 mice per group.

Small-Animal PET Imaging and Image Analysis

Details of the small-animal PET imaging procedure were reported earlier (*20–22*). Briefly, small-animal PET scans were obtained with a microPET R4 rodent-model scanner (Siemens Medical Solutions). Mice were each injected via the tail vein with 2–3 MBq of the ^{18}F-FB-T84.66 diabody under isoflurane anesthesia. The images were reconstructed with a 2-dimensional ordered-subsets expectation maximization algorithm, and no correction was applied for attenuation or scatter (*23*). For each small-animal PET scan, regions of interests (ROIs) were drawn over the tumor and major organs on decay-corrected whole-body coronal images by use of vendor software (ASI Pro 5.2.4.0; Siemens Medical Solutions). On the basis of the assumption of a tissue density of 1 g/mL, the ROIs were converted to MBq/g/min by use of a conversion factor, and the resulting values were divided by the administered activity to obtain an imaging ROI–derived %ID/g.

Statistical Analysis

Quantitative data were expressed as mean ± SD. Means were compared by use of a 1-way ANOVA and the Student *t* test. *P* values of less than 0.05 were considered statistically significant.

RESULTS

Radiolabeling and Radioimmunoreactivity

^{18}F-SFB was synthesized inside the fully automatic module with a decay-corrected radiochemical yield of 32.50% ± 5.92% in 138 ± 8 min ($n = 4$). The radiochemical purity of ^{18}F-SFB was greater than 98%, as determined by analytic HPLC, and the specific activity of ^{18}F-SFB was estimated by radio-HPLC to be 200–250 TBq/mmol (*24,25*). Starting from ^{18}F-SFB, the radiolabeling process took 35 ± 5 min, and the overall radiochemical yield with decay correction was 1.40% ± 0.16% ($n = 4$). The low ^{18}F-labeling yield was likely attributable to the limited number of accessible lysine residues on the diabody surface. The specific activity of the ^{18}F-FB-T84.66 diabody was 1.83 ± 1.71 TBq/mmol. The ^{18}F-FB-T84.66 diabody was well separated from the nonreactive ^{18}F-SFB (eluting after 6 mL), as indicated by the size-exclusion chromatography separation profile shown in Figure 1C. Only the fractions from 3.5 to 5 mL were used for in vitro and in vivo experiments. Radioimmunoreactivity for LS 174T cells was determined to be 57.1% ± 2.0% ($n = 4$), higher than the value of 42% previously reported for the ^{124}I-T84.66 diabody (*8*). For CEA-negative C6 cells, binding was 6.3% ± 1.6% ($n = 4$) under the same conditions, indicating minimal nonspecific binding.

Biodistribution

The biodistribution of the ^{18}F-FB-T84.66 diabody was determined in athymic nude mice bearing LS 174T tumors; the results are shown in Figure 2. As early as 1 h after injection, LS 174T tumor uptake (2.67 ± 1.05 %ID/g) was higher than uptake in any organ except the liver (6.33 ± 1.76 %ID/g), the kidneys (17.16 ± 1.19 %ID/g), and the spleen (8.22 ± 2.49 %ID/g). The tracer was excreted mainly through the renal pathway. Activity accumulation in the kidneys decreased significantly from 1 to 2 h after injection (4.50 ± 0.73 %ID/g; $P < 0.01$) because of the excretion of the tracer into the urinary bladder. All other major organs exhibited background levels of tracer uptake at all time points examined. The blood activity concentration of the tracer at 1 h after injection (2.08 ± 0.49 %ID/g) reflected the blood-pool activity of the tracer, and the uptake decreased significantly at 2 h after injection (0.91 ± 0.21 %ID/g; $P < 0.01$, compared with that at 1 h after injection), indicating the rapid blood clearance of the diabody-based tracer. Although the tracer uptake in all organs decreased over time, LS 174T tumor uptake remained steady. There was no significant difference between LS 174T tumor uptake values at any 2 consecutive time points ($P > 0.05$ in all cases). Because of the rapid blood clearance, the tumor-to-blood ratio increased significantly over time (1.31 ± 0.59,

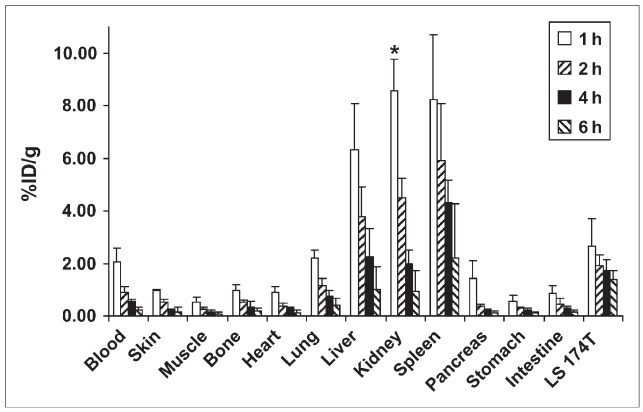

FIGURE 2. Biodistribution of ^{18}F-FB-T84.66 diabody in athymic nude mice bearing LS 174T tumors at several time points after injection ($n = 4$). Note that kidney uptake at 1 h after injection (*) was plotted as half actual value.

2.20 ± 0.71, 3.24 ± 1.21, and 6.78 ± 2.26 at 1, 2, 4, and 6 h after injection, respectively; $P < 0.05$ in all cases). The tumor-to-muscle ratio also increased steadily over time (5.41 ± 2.30, 8.71 ± 5.72, 13.98 ± 8.29, and 29.52 ± 12.61 at 1, 2, 4, and 6 h after injection, respectively). In summary, the ^{18}F-FB-T84.66 diabody exhibited high contrast for LS 174T tumors because of the high binding avidity and the rapid blood clearance from the circulation mainly through the renal pathway and also, to a lesser degree, the hepatic pathway.

Small-Animal PET Imaging

Small-animal PET scans were obtained for the ^{18}F-FB-T84.66 diabody with both the LS 174T tumor model (high CEA expression) and the C6 tumor model (negative for CEA expression) (3 mice per group). Selected coronal images at different time points after injection are shown in Figure 3A. High LS 174T tumor activity accumulation was observed as early as 5 min after injection (data not shown), and high-contrast PET images were obtained as early as 30 min after injection. As shown in Figure 3B, LS 174T tumor uptake remained steady over time (2.55 ± 0.22, 2.37 ± 0.30, 2.22 ± 0.50, and 2.23 ± 0.17 %ID/g at 30 min, 1 h, 2 h, and 4 h after injection, respectively), corroborating the biodistribution results. C6 tumor uptake was at the background level (0.90 ± 0.14, 0.71 ± 0.10, 0.53 ± 0.05, and 0.36 ± 0.15 %ID/g at 30 min, 1 h, 2 h, and 4 h after injection, respectively) and was significantly lower than LS 174T tumor uptake at all time points examined ($P < 0.05$ in all cases) (Fig. 3B). Tracer uptake in the liver, kidneys, and muscle also correlated well with the biodistribution results. Prominent activity in the kidneys and the urinary bladder confirmed the renal clearance pathway of the ^{18}F-FB-T84.66 diabody. Serial small-animal PET imaging studies obtained with the LS 174T and C6 tumor models clearly demonstrated the CEA-targeting avidity and specificity of the ^{18}F-FB-T84.66 diabody in vivo. From the results shown in Figure 3, it can be concluded that 1 h after injection is the optimal time point for

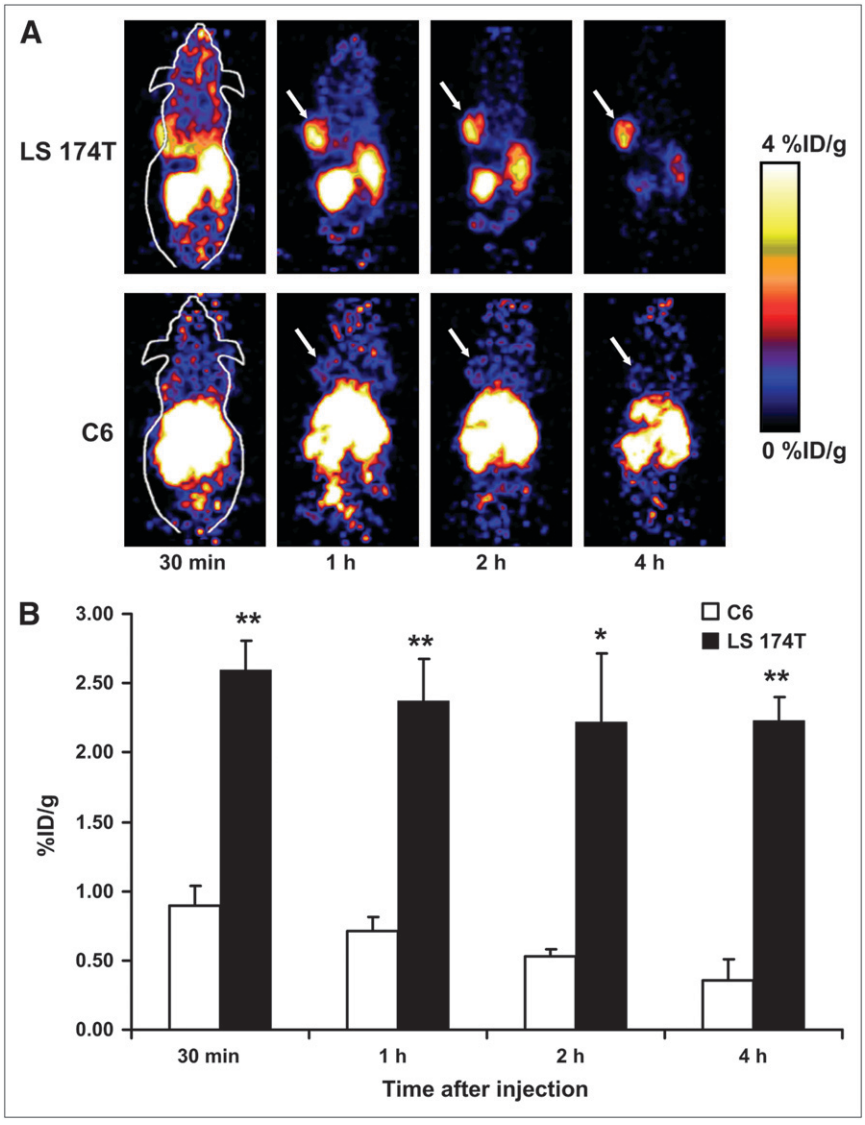

FIGURE 3. (A) Dynamic small-animal PET scans obtained for ^{18}F-FB-T84.66 diabody with LS 174T tumor–bearing mice and C6 tumor–bearing mice. Coronal whole-body slices that contained tumors are shown; arrows indicate tumors. (B) Comparison of LS 174T tumor uptake and C6 tumor uptake. Values were determined from ROI analysis of small-animal PET imaging data. Differences were significant at all time points examined. *$P < 0.05$; **$P < 0.01$.

high-contrast PET imaging of tumors, as the tumor uptake had already reached a maximum and the tracer had largely been cleared from the nontargeted organs.

DISCUSSION

This study demonstrates the feasibility of radiolabeling small, tumor-specific antibody fragments with ^{18}F for PET of cancer. Labeling of the anti-CEA T84.66 diabody was accomplished in 35 ± 5 min from ^{18}F-SFB, a routinely synthesized ^{18}F-labeling prosthetic group used in our laboratory (*17–19,24–26*). Immunoreactivity with CEA-positive LS 174T cells after ^{18}F labeling was comparable to that achieved with ^{124}I- and ^{64}Cu-labeled analogs. The resulting ^{18}F-FB-T84.66 diabody is also adequate for small-animal PET imaging of xenograft-bearing mice, showing CEA-specific tumor uptake and retention.

^{18}F remains the radionuclide of choice for clinical PET. It is a pure positron emitter with a half-life of 109.7 min, well suited for routine use in nuclear medicine applications. The broad availability of ^{18}F and the increasing implementation of clinical PET and PET/CT scanners will facilitate the translation of novel PET tracers to the clinic. Labeling of antibodies with positron-emitting radionuclides has been pursued in many arenas. Many groups have described the labeling of intact antibodies and conventional Fab or F(ab′)$_2$ fragments with the positron-emitting isotopes ^{18}F, ^{64}Cu, ^{68}Ga, ^{76}Br, ^{86}Y, ^{94m}Tc, and ^{124}I (*27–35*). More recently, the development of immuno-PET has been extended through the labeling of genetically engineered antibody fragments, such as disulfide-stabilized Fvs, diabodies, *cys*-diabodies, minibodies, and scFv-Fcs, with positron emitters (*8,9,16,36–38*). The combination of a diabody and ^{18}F is particularly attractive because the diabody benefits from bivalent binding in a format that yields the same molecular mass as monovalent Fab′ fragments (e.g., ^{99m}Tc-arcitumomab). As a result, diabodies demonstrate better tumor uptake and retention in preclinical models than do the monovalent fragments (*39*). Furthermore, the physical half-life of ^{18}F is well matched to the biologic half-life of the diabody. Compared with our previously reported ^{124}I-T84.66 diabody, which had an LS 174T/C6 tumor uptake ratio (essentially the tumor-to-background ratio, because C6 tumor uptake was at the background level at all time points examined) of 3.99 ± 0.98 at 4 h after injection in PET (*8*), the ratio for the ^{18}F-FB-T84.66 diabody was significantly higher, at 6.19 ± 0.47 ($P <$ 0.01). In a comparison with a ^{64}Cu-labeled anti-CEA minibody (a slightly larger antibody fragment with a molecular mass of 80 kDa), which had LS 174T/C6 tumor uptake ratios of 2.98 and 2.48 at 5 and 12 h after injection, respectively (*16*), the contrast obtained in PET with the ^{18}F-FB-T84.66 diabody was also much higher. These results suggest that ^{18}F is the optimal radioisotope for PET with diabody-based tracers. The optimal time point for high-contrast imaging of tumors with the ^{18}F-FB-T84.66 diabody appears to be approximately 1 h after injection, as the tumor uptake had already reached a maximum at 1 h after injection and the tracer had largely been cleared from the nontargeted organs.

A reason for using ^{18}F in lieu of ^{124}I as a diabody radiolabel may be theorized by use of the IFOM. This function is based on the rapidity with which a lesion may be distinguished from the blood-pool background (*14,40*). At a given level of confidence, higher IFOM values imply greater speed in determining that tumor uptake is significantly above that of the surrounding blood. Using published murine pharmacokinetic values for an iodinated diabody and an iodinated minibody (*14*), we calculated the IFOM values for 4 possible cases, diabody and minibody with ^{18}F and ^{124}I labels (Fig. 4), and included a correction for the low positron yield of ^{124}I decay. For the diabody, ^{18}F is the superior radiolabel for times before 4 h after injection. Figure 4A shows that PET using ^{18}F-diabody may begin as early as 1 h after injection. The experimental data shown in Figure 3 are consistent with these calculations. Challenges encountered with using ^{124}I as the radiolabel at such early times follow directly from its 23% positron decay efficiency, although it eventually (after many hours) becomes a superior label because of the relatively short half-life of ^{18}F. However, if a nuclear medicine facility wishes to begin imaging shortly after injection, then ^{18}F is clearly superior to ^{124}I as a radiolabel.

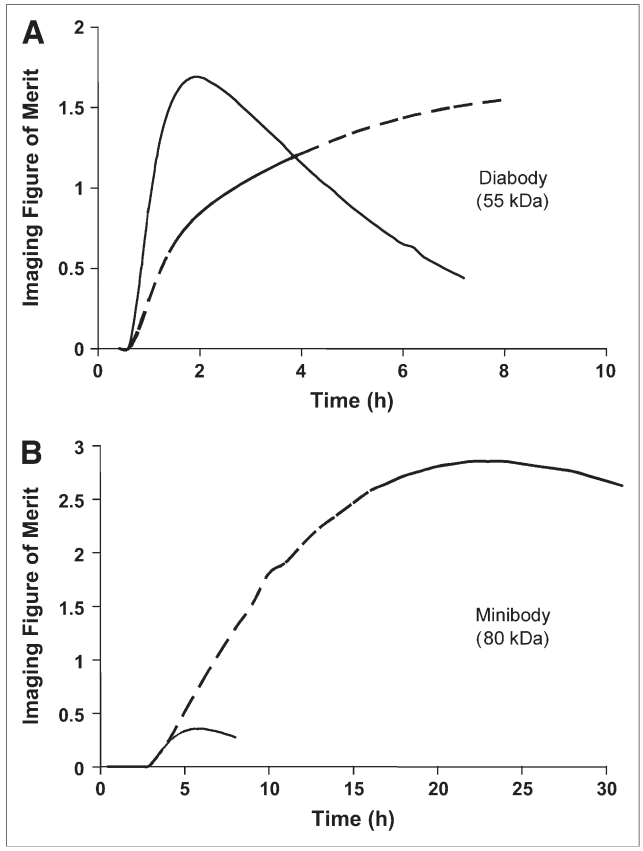

FIGURE 4. IFOM values calculated for anti-CEA diabody (A) and anti-CEA minibody (B) labeled with either ^{18}F (solid lines) or ^{124}I (dashed lines).

Figure 4B shows that a larger fragment, such as a minibody, can be labeled with ^{124}I and that optimal PET imaging should occur at approximately 18–24 h after injection (in agreement with the results of previously published imaging studies). However, the kinetics are too slow for use in combination with ^{18}F (Fig. 4B). Other limitations of using ^{124}I as a PET label include the following: positron range (the average energy of ^{124}I positrons is higher than that of ^{18}F positrons, and the increased positron range would result in a degradation of resolution), decay characteristics (^{124}I has a complex decay scheme, resulting in a high γ-component, with many high-energy γ-emissions occurring in coincidence with each other and with the annihilation photons; these properties complicate the process of quantifying ^{124}I activity in vivo), and availability (^{18}F is readily available in virtually any medical cyclotron facility, whereas ^{124}I production requires high-current solid-state cyclotron targeting and recovery of the target material; therefore, ^{124}I is much less widely available).

The major limitation of the present study that hinders the smooth clinical translation of the ^{18}F-FB-T84.66 diabody is the relatively low labeling yield (less than 2% incorporation). We recently successfully incorporated ^{18}F-SFB synthesis into a commercially available fully automatic synthetic module. Starting from 3.7×10^{10} Bq (1 Ci) of ^{18}F-F$^-$, we can obtain about 3,700–7,400 MBq (100–200 mCi) of purified ^{18}F-SFB within about 2 h from the end of bombardment (decay-corrected radiochemical yield of 20%–40%). Even with this amount of ^{18}F-SFB for diabody coupling, we can obtain only about 55.5–111 MBq (1.5 to 3 mCi) of the ^{18}F-FB-T84.66 diabody for in vivo use, an amount that is sufficient for small-animal studies but that would be too low for clinical applications. The radioimmunoconjugate synthesized this way also has a relatively low specific activity (1.83 ± 1.71 TBq/mmol) compared with those of other reported anti-CEA diabody–based tracers; this property may also be partially responsible for the lower LS 174T tumor uptake of the ^{18}F-FB-T84.66 diabody than that of the ^{124}I-labeled analog. It is unlikely that the low uptake is attributable to the blocking of target sites by unlabeled anti-CEA diabody, as the amount used (about 1 nmol) is far below the level needed to saturate the CEA in the tumor. In order to improve the yield of coupling of ^{18}F-SFB to T84.88 diabody and consequently the specific activity, optimization of reaction conditions is required, and factors such as the diabody–to–^{18}F-SFB activity ratio, reaction temperature, buffer pH, and reaction time will need to be explored.

Our demonstration of successful small-animal PET imaging supports the further development of ^{18}F-labeled antitumor diabodies as a platform for novel PET tracers for clinical cancer detection. Parallel developments in cancer proteomics, target discovery, and target validation, coupled with methods for the rapid production of humanized antibodies (such as phage display and other display technologies as well as transgenic mice that produce human immunoglobulins), will further contribute to this area of PET tracer development.

CONCLUSION

Here we report the ^{18}F labeling of a genetically engineered anti-CEA T84.66 diabody for small-animal PET imaging of colorectal cancer xenografts. The rapid and specific tumor uptake and the fast clearance from the circulation in the mouse xenograft model were observed in both small-animal PET imaging and biodistribution studies. High-contrast small-animal PET images were obtained as early as 1 h after injection of the ^{18}F-FB-T84.66 diabody. This tracer exhibited predominantly renal clearance, with some activity in the liver and spleen at early time points. The ^{18}F-labeled diabody represents a new class of tumor-specific probes for PET based on cell surface antigen expression. The relatively short half-life of ^{18}F is optimal for diabody labeling, because the diabody retains the antigen specificity and affinity of intact antibodies but demonstrates much faster tumor accumulation and blood clearance. The ^{18}F-FB-T84.66 diabody may have great potential as a PET tracer for CEA-producing malignancies.

ACKNOWLEDGMENTS

This work was supported, in part, by the National Institute of Biomedical Imaging and Bioengineering (NIBIB) (R21 EB001785), the National Cancer Institute (NCI) (R21 CA102123, P50 CA114747, U54 CA119367, and R24 CA93862), the Department of Defense (DOD) (W81XWH-04-1-0697, W81XWH-06-1-0665, W81XWH-06-1-0042, and DAMD17-03-1-0143), and a Benedict Cassen Postdoctoral Fellowship from the Education and Research Foundation of the Society of Nuclear Medicine. In addition, support was provided by NCI grant P01 CA43904 and the UCLA Center for In Vivo Imaging in Cancer Biology (P50 CA86306). One of the authors is a member of the UCLA Jonsson Comprehensive Cancer Center (NCI CA16042). Dr. David Dick is acknowledged for ^{18}F-F$^-$ production, and Dr. Frederick T. Chin is acknowledged for synthetic module modification.

REFERENCES

1. Wu AM, Senter PD. Arming antibodies: prospects and challenges for immunoconjugates. *Nat Biotechnol.* 2005;23:1137–1146.
2. Holliger P, Hudson PJ. Engineered antibody fragments and the rise of single domains. *Nat Biotechnol.* 2005;23:1126–1136.
3. Kenanova V, Wu AM. Tailoring antibodies for radionuclide delivery. *Expert Opin Drug Deliv.* 2006;3:53–70.
4. Wu AM, Chen W, Raubitschek A, et al. Tumor localization of anti-CEA single-chain Fvs: improved targeting by non-covalent dimers. *Immunotechnology.* 1996; 2:21–36.
5. Wu AM, Williams LE, Zieran L, et al. Anti-carcinoembryonic antigen (CEA) diabody for rapid tumor targeting and imaging. *Tumor Targeting.* 1999;4:47–58.
6. Viti F, Tarli L, Giovannoni L, Zardi L, Neri D. Increased binding affinity and valence of recombinant antibody fragments lead to improved targeting of tumoral angiogenesis. *Cancer Res.* 1999;59:347–352.
7. Nielsen UB, Adams GP, Weiner LM, Marks JD. Targeting of bivalent anti-ErbB2 diabody antibody fragments to tumor cells is independent of the intrinsic antibody affinity. *Cancer Res.* 2000;60:6434–6440.
8. Sundaresan G, Yazaki PJ, Shively JE, et al. ^{124}I-labeled engineered anti-CEA minibodies and diabodies allow high-contrast, antigen-specific small-animal PET imaging of xenografts in athymic mice. *J Nucl Med.* 2003;44:1962–1969.

9. Robinson MK, Doss M, Shaller C, et al. Quantitative immuno-positron emission tomography imaging of HER2-positive tumor xenografts with an iodine-124 labeled anti-HER2 diabody. *Cancer Res.* 2005;65:1471–1478.
10. Santimaria M, Moscatelli G, Viale GL, et al. Immunoscintigraphic detection of the ED-B domain of fibronectin, a marker of angiogenesis, in patients with cancer. *Clin Cancer Res.* 2003;9:571–579.
11. Wong JY, Chu DZ, Williams LE, et al. Pilot trial evaluating an ^{123}I-labeled 80-kilodalton engineered anticarcinoembryonic antigen antibody fragment (cT84.66 minibody) in patients with colorectal cancer. *Clin Cancer Res.* 2004;10:5014–5021.
12. Krupey J, Gold P, Freedman SO. Purification and characterization of carcinoembryonic antigens of the human digestive system. *Nature.* 1967;215:67–68.
13. Hammarstrom S. The carcinoembryonic antigen (CEA) family: structures, suggested functions and expression in normal and malignant tissues. *Semin Cancer Biol.* 1999;9:67–81.
14. Williams LE, Wu AM, Yazaki PJ, et al. Numerical selection of optimal tumor imaging agents with application to engineered antibodies. *Cancer Biother Radiopharm.* 2001;16:25–35.
15. Yazaki PJ, Shively L, Clark C, et al. Mammalian expression and hollow fiber bioreactor production of recombinant anti-CEA diabody and minibody for clinical applications. *J Immunol Methods.* 2001;253:195–208.
16. Wu AM, Yazaki PJ, Tsai S, et al. High-resolution microPET imaging of carcinoembryonic antigen-positive xenografts by using a copper-64-labeled engineered antibody fragment. *Proc Natl Acad Sci U S A.* 2000;97:8495–8500.
17. Chen X, Park R, Hou Y, et al. microPET imaging of brain tumor angiogenesis with ^{18}F-labeled PEGylated RGD peptide. *Eur J Nucl Med Mol Imaging.* 2004;31:1081–1089.
18. Cai W, Zhang X, Wu Y, Chen X. A thiol-reactive ^{18}F-labeling agent, *N*-[2-(4-^{18}F-fluorobenzamido)ethyl]maleimide, and synthesis of RGD peptide–based tracer for PET imaging of $\alpha_v\beta_3$ integrin expression. *J Nucl Med.* 2006;47:1172–1180.
19. Zhang X, Xiong Z, Wu Y, et al. Quantitative PET imaging of tumor integrin $\alpha_v\beta_3$ expression with ^{18}F-FRGD2. *J Nucl Med.* 2006;47:113–121.
20. Chen X, Hou Y, Tohme M, et al. Pegylated Arg-Gly-Asp peptide: ^{64}Cu labeling and PET imaging of brain tumor $\alpha_v\beta_3$-integrin expression. *J Nucl Med.* 2004; 45:1776–1783.
21. Wu Y, Zhang X, Xiong Z, et al. microPET imaging of glioma integrin $\alpha_v\beta_3$ expression using ^{64}Cu-labeled tetrameric RGD peptide. *J Nucl Med.* 2005;46: 1707–1718.
22. Chen X, Sievers E, Hou Y, et al. Integrin $\alpha_v\beta_3$-targeted imaging of lung cancer. *Neoplasia.* 2005;7:271–279.
23. Visvikis D, Cheze-LeRest C, Costa DC, Bomanji J, Gacinovic S, Ell PJ. Influence of OSEM and segmented attenuation correction in the calculation of standardised uptake values for [^{18}F]FDG PET. *Eur J Nucl Med.* 2001;28:1326–1335.
24. Chen X, Park R, Tohme M, Shahinian AH, Bading JR, Conti PS. microPET and autoradiographic imaging of breast cancer α_v-integrin expression using ^{18}F- and ^{64}Cu-labeled RGD peptide. *Bioconjug Chem.* 2004;15:41–49.
25. Zhang X, Cai W, Cao F, et al. ^{18}F-labeled bombesin analogs for targeting GRP receptor-expressing prostate cancer. *J Nucl Med.* 2006;47:492–501.
26. Chen X, Park R, Shahinian AH, et al. ^{18}F-labeled RGD peptide: initial evaluation for imaging brain tumor angiogenesis. *Nucl Med Biol.* 2004;31:179–189.
27. Garg PK, Garg S, Zalutsky MR. Fluorine-18 labeling of monoclonal antibodies and fragments with preservation of immunoreactivity. *Bioconjug Chem.* 1991;2: 44–49.
28. Otsuka FL, Welch MJ, Kilbourn MR, Dence CS, Dilley WG, Wells SA Jr. Antibody fragments labeled with fluorine-18 and gallium-68: in vivo comparison with indium-111 and iodine-125-labeled fragments. *Int J Rad Appl Instrum B.* 1991;18:813–816.
29. Anderson CJ, Connett JM, Schwarz SW, et al. Copper-64-labeled antibodies for PET imaging. *J Nucl Med.* 1992;33:1685–1691.
30. Bakir MA, Eccles SA, Babich JW, et al. c-erbB2 protein overexpression in breast cancer as a target for PET using iodine-124-labeled monoclonal antibodies. *J Nucl Med.* 1992;33:2154–2160.
31. Larson SM, Pentlow KS, Volkow ND, et al. PET scanning of iodine-124-3F9 as an approach to tumor dosimetry during treatment planning for radioimmunotherapy in a child with neuroblastoma. *J Nucl Med.* 1992;33:2020–2023.
32. Griffiths GL, Goldenberg DM, Roesch F, Hansen HJ. Radiolabeling of an anti-carcinoembryonic antigen antibody Fab′ fragment (CEA-Scan) with the positron-emitting radionuclide Tc-94m. *Clin Cancer Res.* 1999;5(suppl):3001s–3003s.
33. Lovqvist A, Lundqvist H, Lubberink M, Tolmachev V, Carlsson J, Sundin A. Kinetics of ^{76}Br-labeled anti-CEA antibodies in pigs; aspects of dosimetry and PET imaging properties. *Med Phys.* 1999;26:249–258.
34. Lovqvist A, Humm JL, Sheikh A, et al. PET imaging of ^{86}Y-labeled anti–Lewis Y monoclonal antibodies in a nude mouse model: comparison between ^{86}Y and ^{111}In radiolabels. *J Nucl Med.* 2001;42:1281–1287.
35. Smith-Jones PM, Solit DB, Akhurst T, Afroze F, Rosen N, Larson SM. Imaging the pharmacodynamics of HER2 degradation in response to Hsp90 inhibitors. *Nat Biotechnol.* 2004;22:701–706.
36. Choi CW, Lang L, Lee JT, et al. Biodistribution of ^{18}F- and ^{125}I-labeled anti-Tac disulfide-stabilized Fv fragments in nude mice with interleukin 2α receptor-positive tumor xenografts. *Cancer Res.* 1995;55:5323–5329.
37. Olafsen T, Cheung CW, Yazaki PJ, et al. Covalent disulfide-linked anti-CEA diabody allows site-specific conjugation and radiolabeling for tumor targeting applications. *Protein Eng Des Sel.* 2004;17:21–27.
38. Kenanova V, Olafsen T, Crow DM, et al. Tailoring the pharmacokinetics and positron emission tomography imaging properties of anti-carcinoembryonic antigen single-chain Fv-Fc antibody fragments. *Cancer Res.* 2005;65:622–631.
39. Adams GP, Schier R, McCall AM, et al. Prolonged in vivo tumour retention of a human diabody targeting the extracellular domain of human HER2/neu. *Br J Cancer.* 1998;77:1405–1412.
40. Williams LE, Liu A, Wu AM, et al. Figures of merit (FOMs) for imaging and therapy using monoclonal antibodies. *Med Phys.* 1995;22:2025–2027.

JNM The Journal of NUCLEAR MEDICINE

PET Imaging of Colorectal Cancer in Xenograft-Bearing Mice by Use of an ^{18}F-Labeled T84.66 Anti–Carcinoembryonic Antigen Diabody

Weibo Cai, Tove Olafsen, Xianzhong Zhang, Qizhen Cao, Sanjiv S. Gambhir, Lawrence E. Williams, Anna M. Wu and Xiaoyuan Chen

J Nucl Med. 2007;48:304-310.

The Journal of Nuclear Medicine is published monthly.
SNMMI | Society of Nuclear Medicine and Molecular Imaging
1850 Samuel Morse Drive, Reston, VA 20190.
(Print ISSN: 0161-5505, Online ISSN: 2159-662X)

SNMMI SOCIETY OF NUCLEAR MEDICINE AND MOLECULAR IMAGING